A Temperature-Dependent Constitutive Model for Relaxor Ferroelectrics

Ralph C. Smith
Center for Research in Scientific Computation
Department of Mathematics
North Carolina State University
Raleigh, NC 27695-8205
rsmith@eos.ncsu.edu

Craig L. Hom
Advanced Technology Center
Lockheed Martin Missiles & Space
Palo Alto, CA 94304
craig.hom@lmco.com

Abstract

This paper addresses the development of a temperature-dependent constitutive model for relaxor ferroelectric materials. These compounds exhibit a diffuse transition region between the paraelectric and ferroelectric phases due to the chemical heterogeneity of the materials. At low temperatures, the materials exhibit significant dielectric hysteresis in the relation between the applied field E and the macroscopic polarization P, with the degree of hysteresis decreasing as the temperature increases to the freezing temperature T_f. Above the freezing temperature, the relation is single-valued but nonlinear.

These phenomena are modeled by assuming that the material is comprised of an aggregate of micropolar regions having a range of Curie temperatures. Thermodynamic principles are employed to obtain a micropolar model which predicts the saturation polarization and distribution of regions as a function of temperature. A corresponding macroscopic model is then constructed to predict the dielectric behavior of the material above the freezing temperature. Hysteresis below the freezing point is incorporated through the quantification of energy required to bend and translate domain walls pinned at inclusions inherent to the material. The resulting ODE model quantifies the constitutive nonlinearities and hysteresis exhibited by the materials through a wide range of temperatures and input drive levels. The predictive capabilities of the model are illustrated through a comparison with PMN and PMN-PT-BT data collected at temperatures ranging from 133^o K to 313^o K.

1 Introduction

Relaxor ferroelectric compounds are proving advantageous in a number of high performance applications due to their capability for generating large strains with reduced hysteresis when employed at temperatures within their diffuse transition region. For example, a lead magnesium composition $Pb(Mg_{1/3}, Nb_{2/3})O_3$ (PMN-PT) has been demonstrated to produce at least a 6 dB increase in acoustic source levels over Pb(Zr, Ti)O_3 (PZT) when employed as drivers for underwater sonar transducers [12, 15]. The capability of PMN for applications which require micropositioning is illustrated by its success in adaptive optic systems. When employed in multi-layered arrays for deformable mirrors, PMN has increased mirror sensitivity from 0.3 nm/V to 12.0 nm/V relative to monolithic PZT [6, 9, 10].

The stoichiometries and electromechanical mechanisms which provide the materials with superior performance capabilities also imbue them with a complex constitutive behavior which must be quantified to achieve their potential in high performance system design. Throughout the temperature range, the materials exhibit nonlinear saturation effects and positive induced strains due to their electrostrictive nature. Hence they must be biased through an applied field so that they operate in one quadrant of the field-strain curve. The incorporation of the inherent nonlinearities provides the capability for designing tunable sensors once the nonlinearity is characterized. Additionally, the materials exhibit temperature-dependent hysteresis below the freezing temperature with the degree of hysteresis increasing as temperatures decrease as illustrated in Figure 1. Finally, the strains generated by the materials are dependent on both the operating temperature and frequency.

The manner through which these properties are manifested in transducer design can be illustrated through the consideration of a sonar projector. When driven at high fields and high frequency, PMN will heat due to dielectric hysteresis. Since PMN's hysteresis decreases with temperature, actuators reach an equilibrium temperature when heat dissipation due to conduction, convection and radiation balances the internal heat generated by the ceramic. The final equilibrium temperature depends on the configuration of the actuator, its electric drive cycle, and its surrounding environment. Shankar and Hom [16] predicted a 40^o C rise for a flextensional sonar transducer submersed in water using a simple heat generation model for PMN. These predictions agreed quantitatively with experimental measurements made on an actual transducer.

To minimize the deleterious effects of self heating and to optimize the design capabilities of transducers which utilize relaxor ferroelectrics, it is necessary to develop temperature-dependent constitutive relations which quantify the nonlinear behavior and hysteresis throughout the operating range of the materials. The initial models proposed by Hom and Shankar [11] quantified the electrostrictive strains and nonlinear saturation behavior of the materials for isothermal conditions and transition temperatures where hysteresis is negligible. Subsequent experiments by Brown et al. [2] demonstrated that the model accurately pre-

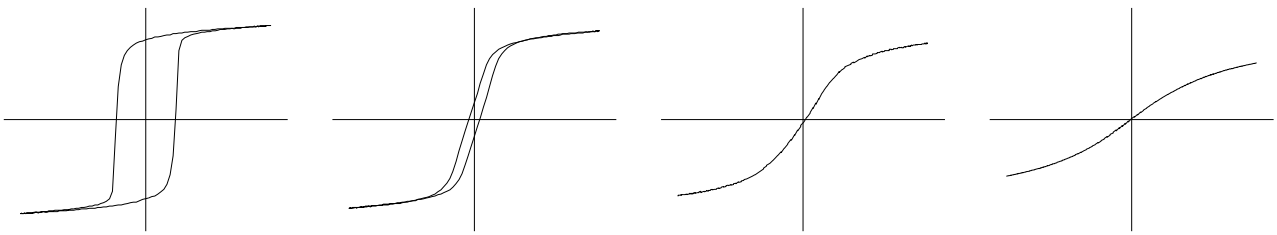

Figure 1. Hysteresis and saturation polarization of PMN as a function of increasing temperature (from Glazounov et al. [7]). Abscissas: electric field (MV/m), ordinates: polarization (C/m^2).

dicts the coupled electromechanical behavior of the materials for isothermal, hysteresis-free (anhysteretic) operating conditions. The hysteresis inherent to the materials at lower temperatures, where the material exhibits a well-defined domain structure, was then modeled by Smith and Hom [19, 20] through the quantification of losses due to domain wall motion. This provided a unified framework which quantified both the nonlinear behavior and hysteresis exhibited by the materials at fixed temperatures and quasistatic operating conditions. An initial model characterizing the temperature-dependence of PMN was developed by Glazounov at al. [7] using as a basis the same polarization model employed by Hom and Shankar. This model focused on the anhysteretic behavior of the materials and was based on the assumption that the material consists of micropolar regions having a distribution of local Curie temperatures. The model quantified the saturation polarization of the aggregate, the density of micropolar regions and the distribution of transition temperatures for PMN but did not account for interactions between polar regions. The theory of Glazounov et al. was subsequently extended by Hom and Shankar [13] to provide a quasistatic, temperature-dependent model for PMN which quantified the nonlinear behavior of the material but did not accommodate the hysteresis present at temperatures below the freezing temperature.

In this paper, we extend the previous theory to provide a unified model which quantifies the temperature-dependent constitutive nonlinearities and hysteresis exhibited by relaxor ferroelectrics from low temperature, ferroelectric regimes through the diffuse transition region preceding their paraelectric state. Like Glazounov et al., we assume that the relaxor material consists of superparaelectric, micropolar regions with a diffuse spectrum of Curie temperatures. However, we use a simple Ising model with near neighbor ion interaction to represent the thermodynamics of the individual micropolar regions. Based on the "random-layer" model of spatial B-site ordering for relaxor ferroelectrics, we calculate the dispersion of local Curie temperatures. The micropolar model predicts the saturation polarization and the density of the polar regions as a function of temperature. A macroscopic model, which includes interaction between the micropolar regions, is then constructed to predict the anhysteretic polarization behavior of the materials above the freezing temperature. The hysteresis inherent to the materials below this temperature is incorporated through the extension of the domain theory in [20] to incorporate thermal dependence in the energy required to translate domain walls. As demonstrated by comparisons to experimental PMN and PMN-PT-BT data, the resulting model accurately quantifies the nonlinear and hysteretic behavior of the materials through a broad temperature range.

The physical mechanisms which provide relaxor ferroelectric materials with their characteristic behavior and a general form of the constitutive equations which quantify this paper are summarized in the remainder of this section. In Section 2, the isothermal anhysteretic and hysteresis models are summarized to illustrate the framework of the model. The fully temperature-dependent model is then developed in Section 3 and illustrated through fits to PMN and PMN-PT-BT data in Section 4. These examples demonstrate the ability of the model to quantify both the hysteretic and anhysteretic behavior of the materials for temperatures ranging from 133^o K to 313^o K.

1.1 Physical Mechanisms for Relaxor Behavior

Normal ferroelectric materials, including the piezoelectric compound PZT, exhibit a sharp ferroelectric to paraelectric phase transition and are operated at temperatures well below this transition. In contrast, relaxor ferroelectrics exhibit a diffuse phase transition over a broad temperature range [5, 7, 23]. Since relaxors are typically employed at temperatures within this transition region, the material's dielectric behavior strongly depends on the temperature and frequency of the applied electric load as illustrated in Figure 2. The transition temperature is often tailored to a specific application by mixing PMN with lead titanate (PT) and additional minor dopants, such as barium titanate (BT) and strontium titanate (ST).

The temperature-dependence of relaxors is manifested in both the degree of hysteresis and the saturation exhibited by the materials as depicted in Figure 1. To be applicable throughout the temperature

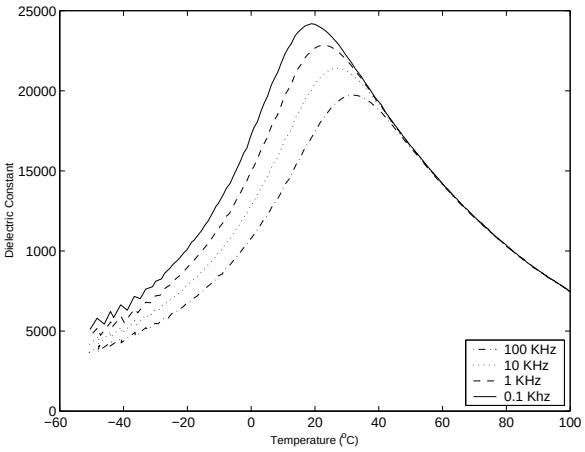

Figure 2. Dielectric response of a PMN-PT-BT (10% PT, 3% BT) at frequencies ranging from 0.1 kHz to 100 Hz.

range, models must accommodate both of these phenomena. Furthermore, Viehland et al. [25, 26] have demonstrated that relaxors deviate from the Curie-Weiss law at temperatures above the temperature of dielectric maximum, T_m, and that they exhibit non-Debye relaxation cumulating in polarization freezing at a temperature below T_m.

To motivate the underlying mechanisms, it is necessary to consider aspects of the stoichiometry of these materials. The PMN compounds have the ABO_3 shown in Figure 3. The A sites are lead anions, while the B sites are a mixture of low valence cations and high valence cations (1/3 Mg^{+2} and 2/3 Nb^{+5} in the case of PMN). The spatial ordering of the multiple B-site cations leads to the diffuse transition of a relaxor. Smolensky postulated a dispersion of cations which creates Mg:Nb rich ferroelectric regions surrounded by pure Nb sites [23]. Each region has a local phase transition, so the aggregate possesses a spectrum of phase transitions. Cross [5] later proposed the more complete picture of relaxor behavior depicted in Figure 4. He postulated that nanoscale size (3-5 nm) polar regions form with decreasing temperature. These small regions have a low energy barrier so they fluctuate with thermal agitation in a manner analogous to superparamagnetism. Each region's dipole moment has random orientation so that the macroscopic polarization is zero but the system's RMS dipole moment is nonzero. Initially, the relaxor obeys the Curie-Weiss relationship with a very high Curie temperature (398^o K for PMN). With

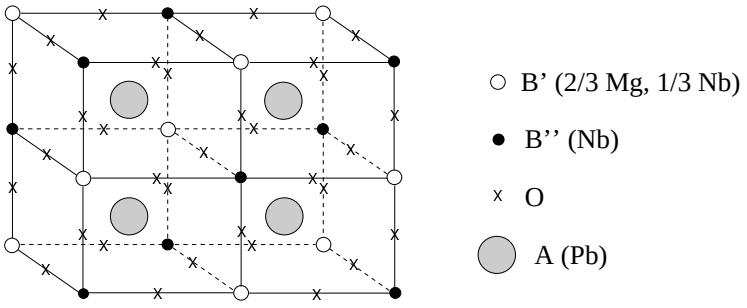

Figure 3. Atomic structure of a perovskite relaxor ferroelectric A(B',B")O_3. The B' and B" sites indicate the cation ordering for the "random layer" model.

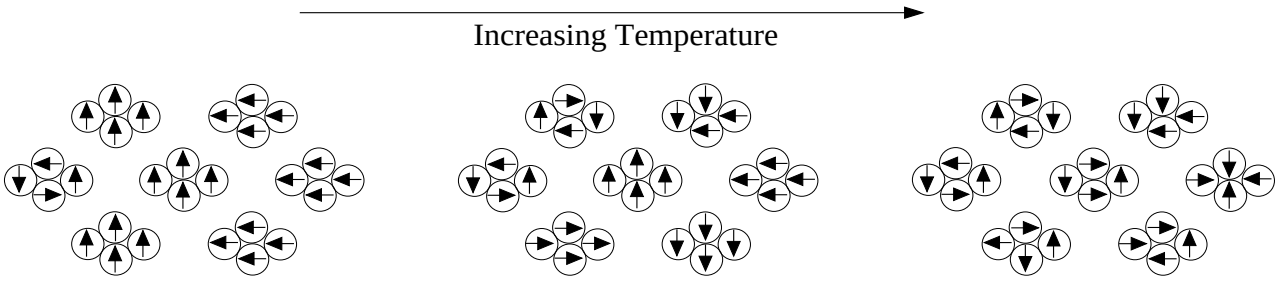

Ferroelectric: The micropolar clusters interact and material exhibits remanent polarization.

Superparaelectric: Micropolar regions develop but have a random orientation due to thermal excitation.

Paraelectric: Micro-regions are nonpolar and material exhibits zero macroscopic polarization.

Figure 4. Polar mechanisms in relaxor ferroelectric materials as postulated by Cross [5]. In the superparaelectric phase, the exhibits a nonzero RMS dipole moment but has zero macroscopic polarization.

further cooling, the thermal fluctuations decrease and interaction between regions freezes the polarization in a manner similar to magnetic spin glasses. The material deviates from the Curie-Weiss relationship and possesses a strong frequency dependence. Eventually, the material develops a permanent remanent polarization and large domains develop as in a normal ferroelectric.

The ordering of the B-site cations plays a crucial role in defining the diffuse nature of the transition and two cation ordering models have been proposed. Diffraction studies indicate that the polar regions have a 1-to-1 distribution of two different cation sites arranged in a face center lattice. These two sites are denoted as B' and B" as depicted in Figure 3. In the "space charge" model for PMN, it is assumed that ordered regions consisting of Mg exclusively occupy the B' sites while Nb exclusively occupies the B" sites [8, 26]. The ordered regions thus carry a net negative charge which should inhibit domain growth. In the "random layer" model [1, 3], Mg and Nb in a 2-to-1 ratio randomly populate the B' sites, while Nb exclusively occupies the B" sites. In this model, the ordered regions are charge-balanced so domains should coarsen during heat treatment. Recent experiments by Akbas and Davies [1] have shown that domain growth does occur during annealing in $Pb(Mg_{1/3}\ Ta_{2/3})O_3$ (PMT), which supports the "random-layer" model of the B-site cation distribution. It is this latter model which we employ in Section 3 when quantifying the macroscopic behavior of the materials.

1.2 General Constitutive Relations

We summarize here the general form of the constitutive relations for relaxor ferroelectric materials. The relation for the direct electrostrictive effect is posed in terms of a general function which is then specified in subsequent sections. To simplify the discussion, we focus on the 1-D case. This provides models which are adequate for a number of applications utilizing relaxors and provides a framework which can be extended to multiaxial models if the application warrants.

To define an appropriate Gibbs function for relaxor materials, we assume that the material is linearly elastic, is electromechanically coupled through electrostrictive effects, and that it exhibits a nonlinear and potentially hysteretic relation between the input field E, the macroscopic polarization P, and the operating temperature T. For polycrystalline materials which are approximately isotropic, an appropriate Gibbs function is

$$G = -\frac{1}{2Y}\sigma^2 - Q_{33}P^2\sigma + \mathcal{G}_0(P,T)$$

where σ denotes the axial stress, Y is the open circuit elastic modulus, Q_{33} is the longitudinal electrostrictive coefficient and $\mathcal{G}_0$ is the stress-free Gibbs free energy. The use of the thermodynamic relations

$$e = -\frac{\partial G}{\partial \sigma} \quad , \quad E = \frac{\partial G}{\partial P}$$

then yields the general constitutive relations

$$\begin{aligned} e &= \frac{1}{Y}\sigma + Q_{33}P^2 \\ E &= -2Q_{33}P\sigma + \mathcal{F}(P,T) \end{aligned} \tag{1}$$

specifying the strain e and field E as functions of the stress, polarization and temperature. The nonlinear map $\mathcal{F}$, which quantifies the stress-free dielectric response of the material, will be specified in subsequent sections.

2 Isothermal Hysteresis Model

To motivate the strategy used to construct the temperature-dependent hysteresis model and constitutive relations, we summarize first the model developed in [19, 20] for fixed temperature applications. The fixed temperature model is constructed in two steps: (1) the characterization of the hysteresis-free (anhysteretic) relation between the input field E and polarization P, and (2) the modeling of hysteresis losses through the quantification of energy required to bend and translate domain walls pinned at inclusions in the material. We note that while the anhysteretic model can be multivalued for certain parameter choices, the transition between saturation values is typically steeper than that observed in polycrystalline materials as temperatures approach the Curie point. The inclusion of domain wall loss mechanisms modulates the transition and provides accurate predictions for the polarization at a range of fixed temperatures. An important attribute of the model is the property that parameters can be asymptotically correlated to physical properties of the data including the coercive field and remanence point, and pertinent asymptotic relations from [21] are summarized at the end of the section to motivated components of the temperature-dependent model developed in Section 3.

Anhysteretic Polarization

The anhysteretic polarization at a given field level E is defined to be the polarization that results when a decaying AC field centered at E is applied to the material. For a fixed stress, it represents an equilibrium between the thermal and electrostatic energies and can thus be modeled using Boltzmann principles. Under the assumption that dipoles can orient only in the direction of the applied field, or opposite to it, the balance of energy yields the Ising spin model

$$P_{an} = p_0 \mathcal{N} \tanh\left(\frac{p_0 E}{k_B T}\right) \tag{2}$$

where p_0 is the dipole moment of a single cell and $\mathcal{N}$ is the total number of moments per unit volume ($\mathcal{N} = N/V$). The thermal energy is quantified by $k_B T$ where k_B is Boltzmann's constant and T is the temperature.

To complete the model for the anhysteretic polarization, it is necessary to incorporate interactions due to neighboring dipoles. These effects, which are analogous to the Weiss fields in magnetic materials, are modeled under the assumption that the effective field at the domain level has the form

$$E_e = E + \alpha P + P_\sigma \, . \tag{3}$$

The component αP incorporates the effects of interdomain coupling while P_σ quantifies the electromechanical coupling due to applied stresses. Finally, to guarantee that the model saturates to the saturation polarization P_s, it is necessary to define

$$P_s = p_0 \mathcal{N} .$$

For regimes in which the electromechanical coupling is adequately modeled by the bilinear relation $P_\sigma = 2Q_{33}P\sigma$, the field can then be expressed as

$$E = -2Q_{33}P\sigma - \alpha P + \frac{k_B N T}{V P_s} \text{arctanh}(P/P_s) . \tag{4}$$

The function $\mathcal{F}$ in (1) is this given by

$$\mathcal{F}(P,T) = -\alpha P + \frac{k_B N T}{V P_s} \text{arctanh}(P/P_s) . \tag{5}$$

For implementation purposes, it is advantageous to express the anhysteretic polarization as

$$P_{an} = P_s \tanh\left(\frac{E_e}{a}\right) \tag{6}$$

where $a = \frac{k_B T}{p_0}$, like α and P_s, is a macroscopic parameter which is estimated using either the asymptotic relations developed in [21] or through a least squares fit to data. We note that while a form of temperature-dependence is incorporated in the parameter a, it does not provide a complete characterization of the thermal behavior of relaxor ferroelectrics through their full operating range. The parameters α and P_s also vary with temperature, and appropriate expressions quantifying the thermal dependence of all three parameters are developed in Section 3.

For certain materials, the assumption that dipoles orient either with or against the field is too stringent and produces models which saturate too quickly. The less restrictive assumption that dipoles can orient uniformly yields the Langevin relation

$$P_{an} = P_s \left[\coth\left(\frac{E_e}{a}\right) - \left(\frac{a}{E_e}\right)\right] \tag{7}$$

when the thermal and electrostatic energies are balanced through Boltzmann relations. The anhysteretic model (7) can provide slightly improved accuracy when characterizing certain materials but it cannot be inverted to yield polarization-based constitutive relations comparable to (4). Both the Ising spin expression (6) and Langevin relation (7) have been employed when modeling the anhysteretic behavior of ferroelectric and ferromagnetic materials.

Hysteresis Model

The second component of the model quantifies the energy required to translate and bend domain walls pinned at inclusions in the material. As detailed in [19, 20], the irreversible changes in polarization due to domain wall translation are incorporated through the quantification of the energy

$$\mathcal{E}_{pin}(P) = k \int_0^P dP$$

required to reorient dipole moments. The parameter k is defined by $k = \frac{n\langle \mathcal{E}_\pi \rangle}{2p}$ where n denotes the average density of pinning sites, p is an average dipole moment, and $\langle \mathcal{E}_\pi \rangle$ is the average energy for 180^o domain walls. While k was considered constant in the fixed-temperature analysis of [19, 20, 21], it is clearly temperature-dependent due to the dependence of $\langle \mathcal{E}_\pi \rangle$ on the thermal energy.

A balance of electrostatic energy then yields the relation

$$\frac{dP_{irr}}{dE} = \widetilde{\delta}\frac{P_{an} - P_{irr}}{k\delta - \alpha\,(P_{an} - P_{irr})} \tag{8}$$

for the irreversible polarization. The parameter $\delta = \text{sign}(E)$ ensure that the energy required to break pinning sites always opposes changes in the polarization. The physical observation that polarization changes after a reversal in field direction are reversible motivates the incorporation of the parameter $\widetilde{\delta}$ which is defined to 1 if $\{dE < 0 \text{ and } P > P_{an}\}$ or $\{dE > 0 \text{ and } P < P_{an}\}$ and is 0 otherwise. The solution of (8) quantifies the irreversible changes in polarization due to domain wall translations.

The second component of the polarization is the reversible polarization which models the effects of domain wall bending. To a first approximation, this is modeled by the relation

$$P_{rev} = c(P_{an} - P_{irr}) \tag{9}$$

where c is a parameter which is estimated for a given material [19, 20, 21].

The total polarization is given by

$$P = P_{irr} + P_{rev}\,. \tag{10}$$

To implement the model, the effective field for a given field and irreversible polarization level is computed using (3). This effective field value is then employed in either (6) or (7) to compute the corresponding anhysteretic polarization. The subsequent irreversible polarization is determined by numerically integrating (8). The total polarization is then specified by (10).

To specify the functional $\mathcal{F}$ in the general constitutive relations (1), it is necessary for the field to be expressed as a function of the polarization. This can be accomplished only through the solution of a differential or integral equation since this is the form of the model used to quantify the evolving hysteresis. The construction of a consolidated differential equation which facilitates inversion is detailed in [20] and details regarding the solution of the inverted problem is described in [17, 18, 22] in the context of the analogous magnetization model. Hence while one cannot provide an algebraic constitutive relation for the polarization-based field for this hysteresis model, the map between P and E is well-defined as the solution to an evolution equation. The determination of the inverse through the solution of a complementary differential equation also facilitates the construction of inverse compensators for linear control design.

Asymptotic Parameter Relations

The previous model requires the parameters α, a, c, P_s and k. Algorithms for determining initial estimates of these parameters using measured values of the remanence polarization, coercive field, peak polarization and field, and the differential susceptibilities at these points were developed in [21]. We summarize here those asymptotic relations which pertain to the development of the temperature-dependent model.

Let χ_{an} and χ_c respectively denote the differential susceptibilities of the anhysteretic polarization at $E = 0$ and the total polarization at $E = E_c$ as depicted in Figure 5. The slopes of the polarization curve before and after tip reversal are denoted by χ_m^+ and χ_m^-. As developed in [21], estimates of the parameters a, c and k are given by the asymptotic relations

$$a = \frac{P_s}{3\chi_{an}} \tag{11a}$$

$$c = \frac{\chi_m^-}{\chi_m^+} \tag{11b}$$

$$k \approx E_c \quad \text{(For soft materials)}. \tag{11c}$$

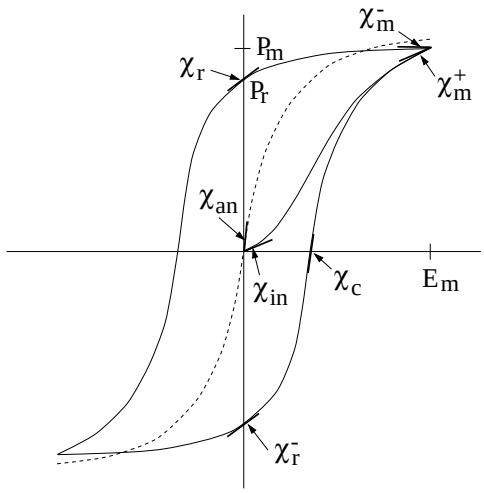

Figure 5. Hysteresis curve with differential susceptibilities employed for parameter determination.

The saturation polarization P_s can quite accurately be estimated directly from high drive level data while the slope χ_{an} is approximated by the slope at coercivity $\chi_{an} \approx \chi_c$. Details concerning these relations as well as the complete algorithm for estimating the full parameter set are provided in [21].

3 Temperature-Dependent Hysteresis Model

From a physical perspective, the parameters a, α, P_s, k and c are temperature-dependent so the model (10) is valid only in operating regimes in which temperatures exhibit minimal variation. In this section we address the temperature-dependence through the consideration of the relaxor ferroelectric as an aggregate of micropolar regions having differing densities of Mg cations and hence differing ferroelectric properties. The development of the anhysteretic relations is motivated by Glazounov et al. [7] and follows the theory developed by Hom and Shankar [13]. The temperature-dependence in the pinning losses is incorporated through energy arguments analogous to those employed in the theory of dislocation plasticity [14]. The combined model can be used to characterize hysteresis in relaxor ferroelectrics throughout a wide range of temperatures encountered in operation.

3.1 Anhysteretic Polarization

As noted previously, relaxor ferroelectrics are assumed to consist of micropolar regions whose transition temperatures and ferroelectric properties are determined by variations in the concentration of cations (Mg^{2+} and Nb^{5+} in PMN) which comprise the material. The anhysteretic component of the model is constructed in two steps. In the first, we consider the thermodynamics of the micropolar regions in order to predict the saturation polarization and density of Mg cations as a function of temperature. Secondly, the interaction between regimes is quantified to construct a macroscopic model which predicts the dielectric properties and polarization of the material for temperatures below the freezing temperature.

For modeling purposes, we make the following assumptions which are depicted in Figure 6.

(i) Each region contains a total of N_0 Mg cations.

(ii) The density of Mg cations X is uniform throughout each region but varies between regions. As a result of Assumption (i), the volume V_i is each region is inversely proportional to X_i.

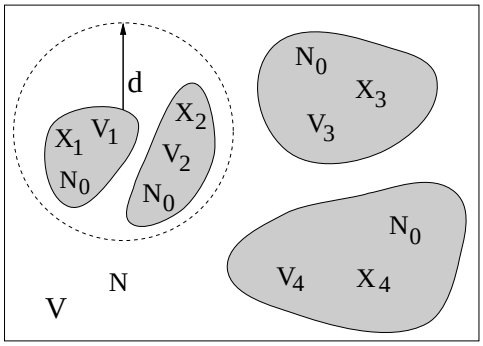

Figure 6. Relaxor ferroelectric consisting of an aggregate of micropolar regions which satisfy Assumptions (i) and (ii). In this depiction, there are $N_R = 4$ regions and a total of $N = N_R N_0$ Mg cations in the material.

(iii) The strength of interactions between regions is directly proportional to the density of nearest neighbors.

(iv) Below its local transition temperature, each region acts as a single dipole and exhibits a remanent polarization.

3.1.1 Thermodynamics of Micropolar Regions

We consider first the behavior of the micropolar regions which is determined by the density of Mg cations which occupy B' sites. Under the assumption that the regions consists of a lattice of cells as depicted in Figure 3, the dipole moment p for the lattice is given by

$$p = p_0 \sum_{i=1}^{N_0} s_i$$

where p_0 is the dipole moment for a single cell and N_0 denotes the number of Mg cations in the region. For PMN, only cells containing a Mg cation possess an associated spin $s_i = \pm 1$ where the sign depends upon the cell's orientation. A correlation between cells is provided by the average

$$R = \frac{1}{N_0} \sum_{i=1}^{N_0} s_i$$

or equivalently, $R = \frac{p}{N_0 p_0}$.

As noted in Assumptions (i) and (ii), we assume that the regions all have the same number N_0 of Mg cations but differing densities and hence volumes. Within a region, we let N_+ and N_- respectively denote the number of positive and negative cells. By noting that $N_0 = N_+ + N_-$, the cell numbers can be expressed in terms of the correlation through the relations

$$\begin{aligned} N_+ &= \frac{N_0}{2}(1+R) \\ N_- &= \frac{N_0}{2}(1-R)\,. \end{aligned} \tag{12}$$

The density X is defined as the number of neighboring B' sites that contain a Mg cation. As indicated by Figure 3, X can range from 1 to 12. Furthermore X is assumed to be uniform throughout the region in accordance with Assumption (ii).

As will be detailed later, the microregions have a distribution of Curie temperatures due to the differing cation densities in the regions. To determine these densities, we note that B' sites have a ratio of 2/3 Mg cations to 1/3 Nb ions. For a Mg populated B' site, each of the 12 adjacent B' sites has a 65.4% probability of being populated by a Mg cation and 34.6% probability of being populated by Nb. The probability that the site is surrounded by X Mg cations is computed by assuming a binomial distribution

$$B(X) = \frac{12!}{X!(12-X)!}(0.654)^X(0.346)^{12-X}\,.$$

To obtain a continuous distribution appropriate for subsequent integration, this was then fit with the normal distribution

$$\Pi(X) = \frac{1}{b\sqrt{2\pi}}e^{-(X-a)^2/2b^2} \tag{13}$$

having a mean $a = 7.85$ and standard deviation $b = 1.65$. Finally, the distribution is normalized to the interval $[0,1]$ through the introduction of the variables

$$\zeta = \frac{X}{12} \quad , \quad \bar{\zeta} = \frac{a}{12} \tag{14}$$

to obtain

$$\Pi(\zeta) = \frac{1}{b\sqrt{2\pi}}e^{-144(\zeta-\bar{\zeta})^2/2b^2}\,. \tag{15}$$

The distributions (13) and (15) will be employed in subsequent discussion to compute ferroelectric properties of the material which depend upon cation densities in the micropolar regions.

To compute the internal energy due to spin conversion, we consider first the energy required to convert an individual spin given a density X of neighboring Mg cations. Letting Φ_0 denote the energy required to convert the spin at a single site when the system is completely ordered ($R = \pm 1$), the energy required to convert a positive spin to negative (and conversely) is given by

$$\begin{aligned} \Phi_{+\to-} &= \frac{X}{12}\frac{N_+}{N_0}\Phi_0 \\ \Phi_{-\to+} &= \frac{X}{12}\frac{N_-}{N_0}\Phi_0\,. \end{aligned} \tag{16}$$

We point out that these energy expressions are derived under the assumption that dipoles interact only with adjacent neighbors.

The change in the internal energy U due to spin conversion can then be expressed as

$$dU = \Phi_{+\to-}dN_- + \Phi_{-\to+}dN_+\,. \tag{17}$$

By utilizing the energy relations (16) and noting from (12) that $dN_+ = \frac{N_0}{2}dR = -dN_-$, the expression (17) can be integrated to obtain the relation

$$U = \frac{\Phi_0 N_0 \zeta}{4}(1-R^2) + U_0\,,$$

where U_0 denotes the energy for the completely ordered state, for the internal energy.

For stress free conditions, the total Gibbs free energy Γ for the microregion is related to the internal energy by

$$\Gamma = U - STV_0$$

where S denotes the entropy and V_0 is the volume of the microregion. From statistical mechanics, the entropy per unit volume for the system can be expressed as

$$S = \frac{k_B N_0}{V_0} \ln[w(R)] = \frac{k_B N_0}{V_0} \ln\left[\begin{pmatrix} N_0 \\ N_+ \end{pmatrix}\right] = \frac{k_B N_0}{V_0} \ln\left[\frac{N_0!}{N_+! N_-!}\right]$$

where $w(R)$ denotes the number of possible spin combinations that yield the correlation R. The entropy expression can be simplified to

$$S = \frac{K_B N_0}{V_0}\left[\ln(2) - \frac{1+R}{2}\ln(1+R) - \frac{1-R}{2}\ln(1-R)\right]$$

which yields the free energy

$$\Gamma = \frac{\Phi_0 N_0 \zeta}{4}(1-R^2) + \frac{k_B N_0 T}{2}\left[R\ln\left(\frac{1+R}{1-R}\right) - \ln(1-R^2)\right] + U_0 + k_B N_0 \ln(2)$$

for the region. We note that the expression for Γ incorporates the ordering of neighboring moments reflected in the first term and the tendency for disorder due to thermal agitation as reflected in the second term.

The electric field E_{loc} in the polar region is determined by

$$p_0 N_0 E_{loc} = \frac{\partial \Gamma}{\partial R} = -\frac{\zeta \Phi_0 R}{2} + T k_B \text{arctanh}(R)\,.$$

In the absence of a local field, the equation can be expressed as

$$R = \frac{T}{T_{cur}}\text{arctanh}(R) \tag{18}$$

where

$$T_{cur} = \frac{\zeta \Phi_0}{2k_B} \tag{19}$$

denotes the local Curie temperature for that region. To motivate the definition (19) and this terminology, it is noted that (18) has a single solution for $T > T_{cur}$ and three solutions comprised of two stable and one unstable solution for temperatures $T < T_{cur}$. Hence a pitchfork bifurcation occurs at $T = T_{cur}$ which is consistent with a second-order phase transition.

The expression (19) quantifies the Curie temperature for a single micropolar region. The macroscopic Curie temperature for the material is specified as the average Curie temperature for the regions or the Curie temperature of the mean,

$$\overline{T}_{cur} = \frac{\bar{\zeta}\Phi_0}{2k_B}\,. \tag{20}$$

The behavior of each polar regions can then be expressed as

$$p_0 N_0 E_{loc} = \frac{\Phi_0}{2}\left[-\zeta R + \frac{\bar{\zeta} T}{\overline{T}_{cur}}\text{arctanh}(R)\right] \tag{21}$$

in the absence of interactions between regions.

3.1.2 Macroscopic Relations

The previous discussion focuses on the thermodynamics within a micropolar region and does not address interactions between regions. As detailed in [20], however, such interactions can significantly affect the effective field present within the material and we focus here on the development of commensurate constitutive relations for the aggregate material which incorporates these effects.

The constitutive relation (4) quantifies the dependence of the field on the polarization for fixed temperatures. To incorporate thermal dependence, it is necessary to quantify the effects of temperature on the number of dipoles N and the coupling coefficient α. As depicted in Figure 6, N is taken to be $N = N_R N_0$ where N_R and N_0 respectively denote the number of micropolar regions and the number of Mg cations in each region. To quantify α, we employ Assumption (iii) from Section 3.1 and assume that the strength of interactions is proportional to the number of neighbors N_d within a distance d of a cluster. Under stress-free anhysteretic conditions, we then propose the constitutive relation

$$E = \frac{-\Phi N_d N_R}{2VP_s^2} P + \frac{k_B T N_R N_0}{VP_s} \text{arctanh}\left(\frac{P}{P_s}\right) \tag{22}$$

for relaxor materials. Here V denotes the volume of material while Φ is a relative measure of the interaction energy between polar regions. We note that the second term on the right side of (22) is proportional to the function employed by Glazounov et al. [7] for non-interacting clusters.

Under the assumption that the clusters are uniformly distributed, the number within a distance d can be expressed as

$$N_d = \frac{4\pi d^3 N_R}{3V}\,.$$

With the definition

$$T_f = \frac{2\pi\Phi d^3 N_R(T_f)}{3k_B V}$$

for the freezing temperature, the temperature-dependent constitutive relation between the field and polarization can then be expressed as

$$E(T) = \frac{2\pi\Phi d^3 N_R}{3V}\left[\frac{-N_R}{VP_s^2}P + \frac{N_0 N_R(T_f)}{P_s V}\frac{T}{T_f}\text{arctanh}\left(\frac{P}{P_s}\right)\right]\,. \tag{23}$$

We now employ the theory developed in Section 3.1.1 for the thermodynamics of the micropolar regions to express P_s and N_R in terms of the operating temperature and parameters which must be estimated for a specific material.

The saturation polarization occurs when the dipole moments in all the microregions are aligned with the field. The degree of alignment for microregions is quantified by the correlation $R(T, X)$ specified by (21) while the magnitude is dependent upon the number $n(X)$ of Mg cations having X nearest neighbors. Recalling that p_0 denotes the dipole moment of a single cell, the saturation polarization can be expressed as

$$P_s(T) = \frac{1}{V}\int_0^{12} |R(T,X)|\, p_0 n(X) dX\,.$$

Since N denotes the total number of Mg cations in the volume V, we can express $n(X) = N\Pi(X)$. Normalization to the unit interval then yields the expression

$$P_s(T) = \widetilde{P}_s \int_0^1 |R(T,\zeta)|\, \Pi(\zeta) d\zeta\,. \tag{24}$$

The distribution Π is computed using (15) and the parameter $\widetilde{P}_s = \frac{Np_0}{V}$ is estimated either directly from the data or through a least squares fit to the data. The correlation R is computed through iterative solution

of the relation

$$\beta E_{loc} = -\zeta R + \frac{\bar{\zeta} T}{\overline{T}_{cur}} \text{arctanh}(R) \tag{25}$$

where $\beta = \overline{\frac{2p_0 N_0}{\Phi_0}}$ denotes the average degree to which local fields turn the polarization and hence change the correlation; see (21). We note that at low drive levels, this contribution is small and one can employ $\beta = 0$. For high drive levels, however, P_s is more accurately approximated by treating β as a parameter to be estimated and solving (25) with $E_{loc} = E_{max}$.

The number of micropolar regions N_R, at a fixed temperature T, is computed by determining those regions with nonzero correlation R, or from (25), those regions in which $T < T_{cur}$. Since the number of regions with density X is given by $n(X)/N_0 = N\Pi(X)/N_0$, the total number of regions in the volume is

$$\frac{N_R(T)}{V} = \frac{N}{VN_0} \int_{\bar{\zeta} T/\overline{T}_{cur}}^{1} 12\Pi(\zeta) d\zeta \, . \tag{26}$$

The use of (24) and (26) in (23) yields the temperature-dependent constitutive relation

$$E = \frac{-2\pi\Phi d^3}{3} \left(\frac{N}{VN_o}\right)^2 \frac{I_1^2(T)}{P_s^2(T)} P + \frac{2\pi\Phi d^3 N_0}{3} \left(\frac{N}{VN_o}\right)^2 \frac{I_2}{T_f} \frac{I_1(T)}{P_s(T)} \text{arctanh}\left(\frac{P}{P_s(T)}\right) \tag{27}$$

where

$$I_1(T) = \int_{\bar{\zeta} T/\overline{T}_{cur}}^{1} 12\Pi(\zeta) \, d\zeta$$

$$I_2 = \int_{\bar{\zeta} T_f/\overline{T}_{cur}}^{1} 12\Pi(\zeta) \, d\zeta \tag{28}$$

$$P_s(T) = \widetilde{P}_s \int_0^1 12|R(T,\zeta)| \, \Pi(\zeta) \, d\zeta \, .$$

For implementation purposes, we formulate (27) as

$$E = \widetilde{\alpha} \frac{I_1^2(T)}{P_s^2(T)} P + \widetilde{a} \frac{I_2}{T_f} \frac{I_1(T)}{P_s(T)} \text{arctanh}\left(\frac{P}{P_s(T)}\right) \tag{29}$$

where $\widetilde{\alpha}$ and $\widetilde{a}$ are parameters which are estimated for a given material through a least squares fit to data. For the subsequent hysteresis model, the constitutive relation is formulated as

$$E = \alpha(T) P + a(T) \text{arctanh}\left(\frac{P}{P_s(T)}\right) \tag{30}$$

with the temperature-dependent parameters

$$\alpha(T) = \widetilde{\alpha} \frac{I_1^2(T)}{P_s^2(T)}$$

$$a(T) = \widetilde{a} \frac{I_2}{T_f} \frac{I_1(T)}{P_s(T)}$$

$$P_s(T) = \widetilde{P}_s \int_0^1 12|R(T,\zeta)| \Pi(\zeta) \, d\zeta$$

where $\widetilde{P}_s = \frac{p_0 N}{V}$ must be estimated for a given material. The resulting model for the anhysteretic polarization is

$$P_{an}(T) = P_s(T) \tanh\left[\frac{E + \alpha(T) P_{an}(T)}{a(T)}\right] \, . \tag{31}$$

3.2 Domain Wall Losses

The anhysteretic model (31) quantifies the polarization which would occur in the absence of domain wall pinning. For certain parameter choices, this model produces a form of hysteresis similar to that observed in a single crystal which undergoes domain switching. However, the transition from remanence to the coercive point is steeper than that observed in most operating regimes. Furthermore, the parameters obtained at temperatures rising to the material's freezing point typically yields a single-valued anhysteretic curve whereas hysteresis is still present in the E-P relation. These phenomena are attributed to energy losses due to domain wall pinning.

As summarized in Section 2, the quantification of the irreversible and reversible polarizations, respectively, requires the parameters k and c. We focus here on the quantification of the temperature-dependence in k since it directly affects the decrease in coercivity observed as temperatures increase to the freezing point. The parameter c is taken as constant since its variation with temperature appears to be secondary. If further refinement is required, analysis of the type developed for k can be extended to include the reversible effects quantified by c.

For fixed temperature, it is noted in Section 2 that through the definition $k = \frac{n\langle \mathcal{E}_\pi \rangle}{2p}$, the parameter k depends on the 180^o domain wall energy $\langle \mathcal{E}_\pi \rangle$ required to move between potential wells. The temperature dependence in k is attributed to the temperature-dependence of the potential wells and hence $\langle \mathcal{E}_\pi \rangle$. To quantify the reduction in energy required to move between wells at increasing temperatures, we employ the asymptotic relation $k \approx E_c$ noted in (11c) and focus initially on the temperature-dependence of the coercive field E_c.

The influence of temperature on the coercive field behavior is predicted using energy arguments drawn from the theory of dislocation plasticity [14] and is similar to the approach employed by Chen and Wang [4]. In this theory, energy barriers ΔG due to local resistive fields $\widehat{E}$ are considered as the mechanism which inhibits domain wall movement and hence prohibits domain wall movement and hence provides potential wells. Using energy arguments analogous to those for slip dislocations, the application of Boltzmann theory yields the modified Arrhenius equation

$$\frac{dP}{dt} = \Delta P_0 \left(\frac{\Delta g}{h} \right) \mu_0 \exp\left(\frac{-\Delta G}{k_B T} \right) \tag{32}$$

for the polarization rate. Here $\mu_0, \Delta g, h$ and ΔP_0 respectively denote the frequency at which the domain wall vibrates, the distance traveled by the wall, the distance between walls, and the local change in polarization due to domain wall movement.

To specify the energy barrier ΔG, we consider the phenomenological model

$$\Delta G = G_0 \left[1 - \left(\frac{E}{\widehat{E}} \right)^{1/p} \right]^q$$

which is analogous to that employed in the theory of dislocation plasticity [14]. The parameter G_0 designates the total free energy required to overcome the obstacle. The parameters p and q quantify the shape of the obstacle as depicted in Figure 7. For the analysis which follows, the choice $q = 1$ with general p proves sufficiently general, and in this case

$$\Delta G = \widehat{G}_0 (E^{1/p} - \widehat{E}^{1/p})$$

where $\widehat{G}_0 = G_0 / \widehat{E}^{1/p}$. We note that in their theory, Chen and Wang employed $p = q = 1$.

For fixed frequencies which are sufficiently low to permit quasistatic approximations, this yields

$$\frac{dP}{dE}\frac{dE}{dt} = p_1 \exp\left[\frac{-\widehat{G}_0 \left(\widehat{E}^{1/p} - E^{1/p} \right)}{k_B T} \right]$$

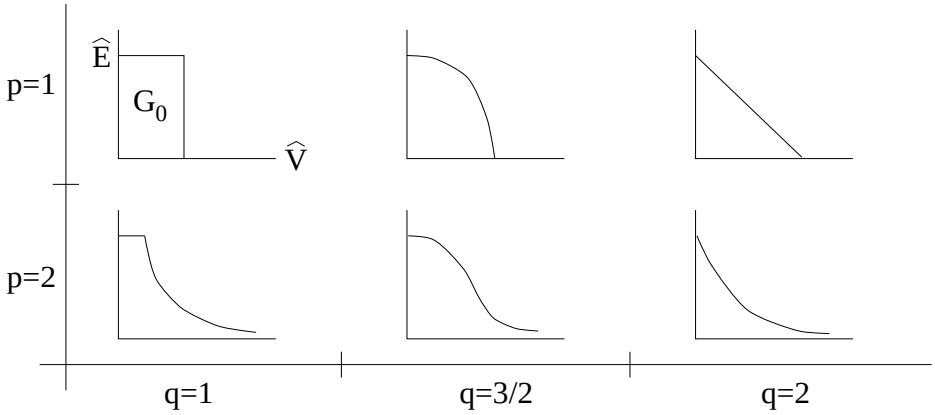

Figure 7. The influence of p and q on the shape of short range obstacles which are sensitive to thermal activation (after [14]).

where $p_1 = \Delta P_0 \Delta g \mu_0 / h$. With the definition $p_2 = \frac{1}{p_1}\frac{dE}{dt}$, it follows that

$$E^{1/p} = T\frac{k_B}{\widehat{G}_0}\ln\left(p_2\frac{dP}{dE}\right) + \widehat{E}^{1/p}\,.$$

Consideration of the coercive field $E = E_c$ then yields

$$E_c^{1/p} = T\frac{k_B}{\widehat{G}_0}\ln\left[p_2\chi_c(T)\right] + \widehat{E}^{1/p} \tag{33}$$

where $\chi_c(T)$ denotes the differential susceptibility at E_c (See Figure 5). The susceptibility will be temperature-dependent since

$$\chi_c(T) \approx \chi_{an}(T) \approx \frac{P_s(T)}{3a(T)}$$

as indicated by the asymptotic relation (11b) of Section 2.2. The contribution $\ln[p_2\chi_c(T)]$ is dominated by T, however, so to a first approximation, we can represent the temperature dependence of the coercive field by

$$E_c = \widetilde{k}(T_f - T)^p \tag{34}$$

where T_f is the freezing temperature where remanence disappears and $\widetilde{k}$ is a material-dependent parameter. We note that for $p = 1$, the expression (34) yields a linear relation between the coercive field and operating temperature which is consistent with the data plotted in Figure 2 of [4] for a variety of materials. At low temperatures, however, one can observe a quadratic dependence as illustrated for PMN in Example 2 of the next section.

Finally, from the asymptotic relation $k \approx E_c$ (see (11c)) for soft materials, we consider the relation

$$k(T) = \widetilde{k}(T_f - T)^p \tag{35}$$

for the pinning constant at temperatures $T < T_f$ where hysteresis is present. For temperatures $T > T_f$, the material exhibits no hysteresis so $k(T) = 0$ and the irreversible relation

$$P_{irr}(T) = P_{an}(T) - \delta\varepsilon_0 k(T)\frac{dP_{irr}}{dD_e}(T)\,, \tag{36}$$

derived in [20] and used to obtain (8), reduces to the anhysteretic model (31).

3.3 Temperature-Dependent Hysteresis Model

The full hysteresis model is constructed in the manner summarized in Section 2 with the temperature-dependent coefficients, developed in Sections 3.1 and 3.2, employed in the models for the anhysteretic, irreversible and reversible polarizations. The parameters, along with the complete model are summarized in Algorithm 1 below. Details regarding the implementation of this algorithm are provided in [20, 21]. Examples illustrating the performance of the model are provided in Section 4.

Algorithm 1:

(A) Determine Temperature-Dependent Parameters

(1) At a specified temperature, estimate $\widetilde{\alpha}, \widetilde{a}, \widetilde{k}, \beta, c, p$ and $\widetilde{P}_s = p_0 N/V$ using the asymptotic relations from [21] or a least squares fit to data. Note that for small drive level applications and moderate temperature ranges, one can often employ $\beta = 0$ and $p = 1$.

(2) Compute the temperature-dependent parameters

$$\begin{aligned} \alpha(T) &= \widetilde{\alpha}\frac{I_1^2(T)}{P_s^2(T)} \quad , \quad P_s(T) = \widetilde{P}_s \int_0^1 12|R(T,\zeta)|\,\Pi(\zeta)\,d\zeta \\ a(T) &= \widetilde{a}\frac{I_2}{T_f}\frac{I_1(T)}{P_s(T)} \quad , \quad k(t) = \widetilde{k}(T_f - T)^p \end{aligned} \tag{37}$$

where

$$I_1(T) = \int_{\bar{\zeta}T/\overline{T}_{cur}}^1 12\Pi(\zeta)\,d\zeta$$

$$I_2 = \int_{\bar{\zeta}T_f/\overline{T}_{cur}}^1 12\Pi(\zeta)\,d\zeta$$

$$\Pi(\zeta) = \frac{1}{b\sqrt{2\pi}} e^{-144(\zeta-\bar{\zeta})^2/2b^2} \quad , \quad \bar{\zeta} = a/12 \ , \ a = 7.85, b = 1.65$$

$$\beta E_{max} = -\zeta R + \frac{\bar{\zeta}T}{\overline{T}}\text{arctanh}(R)$$

(B) Temperature-Dependent Polarization

(1) Construct Anhysteretic Polarization

$$P_{an}(T) = P_s(T)\tanh\left[\frac{E + \alpha(T)P_{irr}(T)}{a(T)}\right]$$

(2) Irreversible Polarization

$$\frac{dP_{irr}}{dE}(T) = \widetilde{\delta}\frac{P_{an}(T) - P_{irr}(T)}{k\delta - \alpha\left[P_{an}(T) - P_{irr}(T)\right]}$$

(3) Reversible Polarization

$$P_{rev}(T) = c[P_{an}(T) - P_{irr}(T)]$$

(4) Total Polarization

$$P(T) = P_{irr}(T) + P_{rev}(T)$$

4 Model Validation

The model derived in Section 3 quantifies the polarization in relaxor ferroelectric materials as a function of both the input field E and the temperature T. To illustrate the performance of the model, we consider both PMN and PMN-PT-BT data over a wide range of temperatures both above and below the freezing temperatures. For each set of data, a single set of parameters was employed throughout the full temperature range, and the temperature and electric field provided the sole inputs to the model. The results illustrate that through the incorporation of associated physics, the model characterizes a wide range of dielectric behavior.

Example 1 (PMN-PT-BT):

We consider first the capability of the model to characterize and predict the dielectric behavior of PMN-PT-BT for input fields having a peak value of 1 MV/m at temperatures ranging from $T = 263^o$ K to $T = 313^o$ K. At the lower temperature, the material exhibits ferroelectric behavior and significant hysteresis as shown in Figure 8. As the temperature increases through the freezing temperature (approximately 288^o K), the hysteresis vanishes and the material exhibits a single-valued superparaelectric relation between the applied field and measured polarization. The data was collected from a stress-free sample ($\sigma = 0$) and the input field was cycled at 1 Hz to maintain quasi-static conditions.

The parameter values $\widetilde{\alpha} = 1.5 \times 10^7, \widetilde{a} = 7.65 \times 10^7, \widetilde{k} = 4.0 \times 10^3, \widetilde{P}_s = 0.53, \beta = 7 \times 10^{-9}, c = .3$ and $p = 1$ were obtained through a least squares fit to the data. The freezing temperature was specified

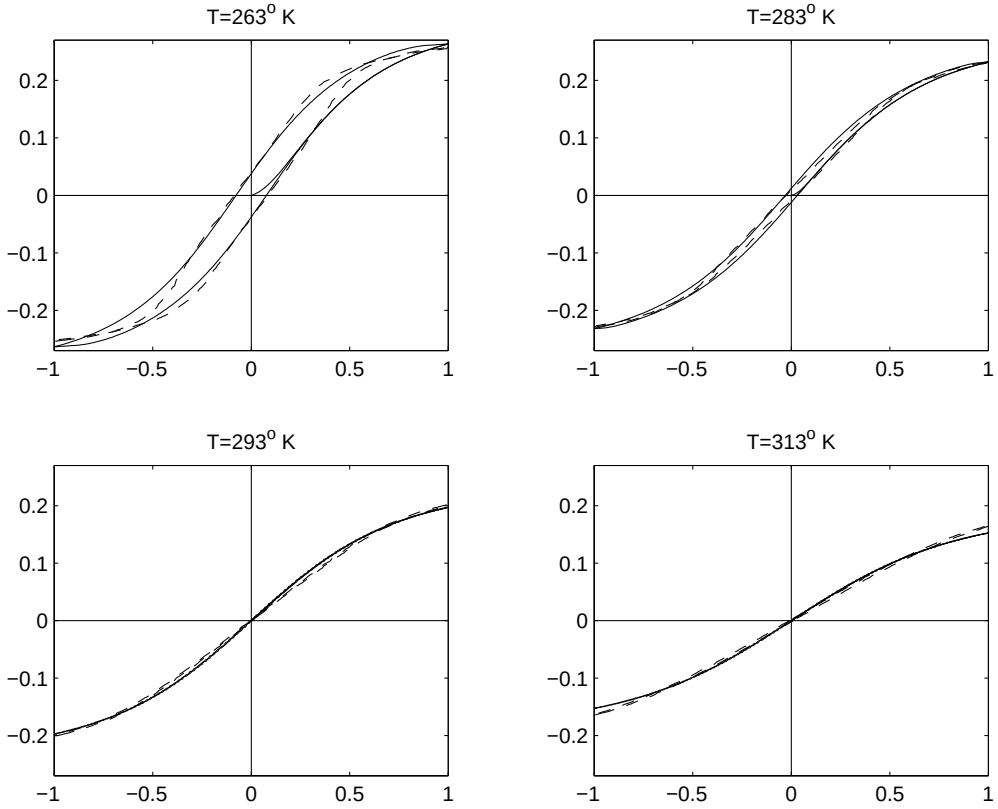

Figure 8. PMN-PT-BT data (– – –) and the domain wall model (——) for the temperature range $T = 263^o$K to $T = 313^o$K. Abscissas: electric field (MV/m), ordinates: polarization (C/m^2).

to be $T_f = 288^o$ K and the Curie temperature was taken to be $\overline{T}_{cur} = 313^o$ K. We reiterate that the temperature-dependence in the parameters $\alpha(T), a(T), k(T)$ and $P_s(T)$ is incorporated solely through the relations (37) and the same parameter set was employed through the full range of temperatures and field inputs.

The model fit obtained with these parameters is compared with the measured data in Figure 8. It is observed that the model very accurately quantifies the initial hysteresis at $T = 263^o$ K, the decreased hysteresis at $T = 283^o$ K, and the anhysteretic behavior at higher temperatures. It also quantifies the decrease in the maximum measured polarization which occurs as temperatures increase. We point out the model parameters were chosen to optimize the model predictions throughout the full temperature range and better fits can be obtained for specific temperature intervals if desired. For example, the parameter choices $\widetilde{\alpha} = 1.4 \times 10^7, \widetilde{a} = 5.74 \times 10^7, \widetilde{k} = 5.0 \times 10^3, \widetilde{P}_s = 0.53$ and $c = .5$ yield a highly accurate model fit to the hysteresis at $T = 263^o$ K but with less accuracy at the higher temperatures.

Example 2 (PMN):

To provide a second illustration of the model attributes over a more extensive temperature range, we consider its capability for predicting the dielectric behavior of PMN data collected by Glazounov et al. [7]. The data set under consideration is plotted in Figure 9. For temperatures ranging from $T = 133^o$ K to $T = 313^o$ K, the input fields were prescribed to have peak values of 3.52 MV/m and frequencies of 0.1 Hz to minimize frequency effects. The data exhibits significant hysteresis in the low temperature ferroelectric regimes with decreasing hysteresis and saturation values as the temperatures increase.

To illustrate the thermal dependence of the hysteresis loss parameter $k(T)$ for this temperature range, the coercive fields are plotted as a function of temperature in Figure 10. Additionally, the best least squares linear and quadratic fits to the data are plotted to motivate the choice of p in the relation

$$k(T) = \widetilde{k}(T_f - T)^p \,,$$

where $k(T) \approx E_c(T)$, derived in Section 3.2. It is observed that for temperatures above 213^o K, the coercive data exhibits a nearly linear dependence on temperature and one can employ $p = 1$ as in Example 1. For the full temperature range, however, a linear model will significantly underestimate the coercive field at low temperatures and a quadratic model is required for accurate predictions; hence for the model development, we employed $p = 2$. Finally, the data in Figure 10 indicates that the critical freezing temperature for this material lies between 233^o K and 253^o K, and we employed $T_f = 242^o$ K in the model.

The bulk Curie temperature was taken to be $\overline{T}_{cur} = 398^o$ K. The remaining model parameters were estimated through a least squares fit to the data. The model predictions obtained with the parameter set $\widetilde{\alpha} = 1.8 \times 10^8, \widetilde{a} = 2.5 \times 10^8, \widetilde{k} = 190, \widetilde{P}_s = 0.38, \beta = 1.42 \times 10^{-8}$ and $c = 0.1$ are compared to the PMN data in Figure 9. It is observed that the model quantifies both the hysteretic dielectric behavior in the ferroelectric regime and the decaying anhysteretic response above the freezing temperature. The primary discrepancy between the data and model predictions lies in the elbow of the hysteresis curve where the model predicts a more gradual transition from saturation to coercivity than is observed in the data. It is hypothesized that this is due to domain rotation mechanisms which are not incorporated in the anhysteretic model. We note that the model fits at any given temperature can be improved by optimizing the parameters for that temperature. However, the specified parameter set provides a good fit throughout the temperature range, with thermal dependence in $\alpha(T), a(T), k(T)$ and $P_s(T)$ incorporated solely through the expressions (37).

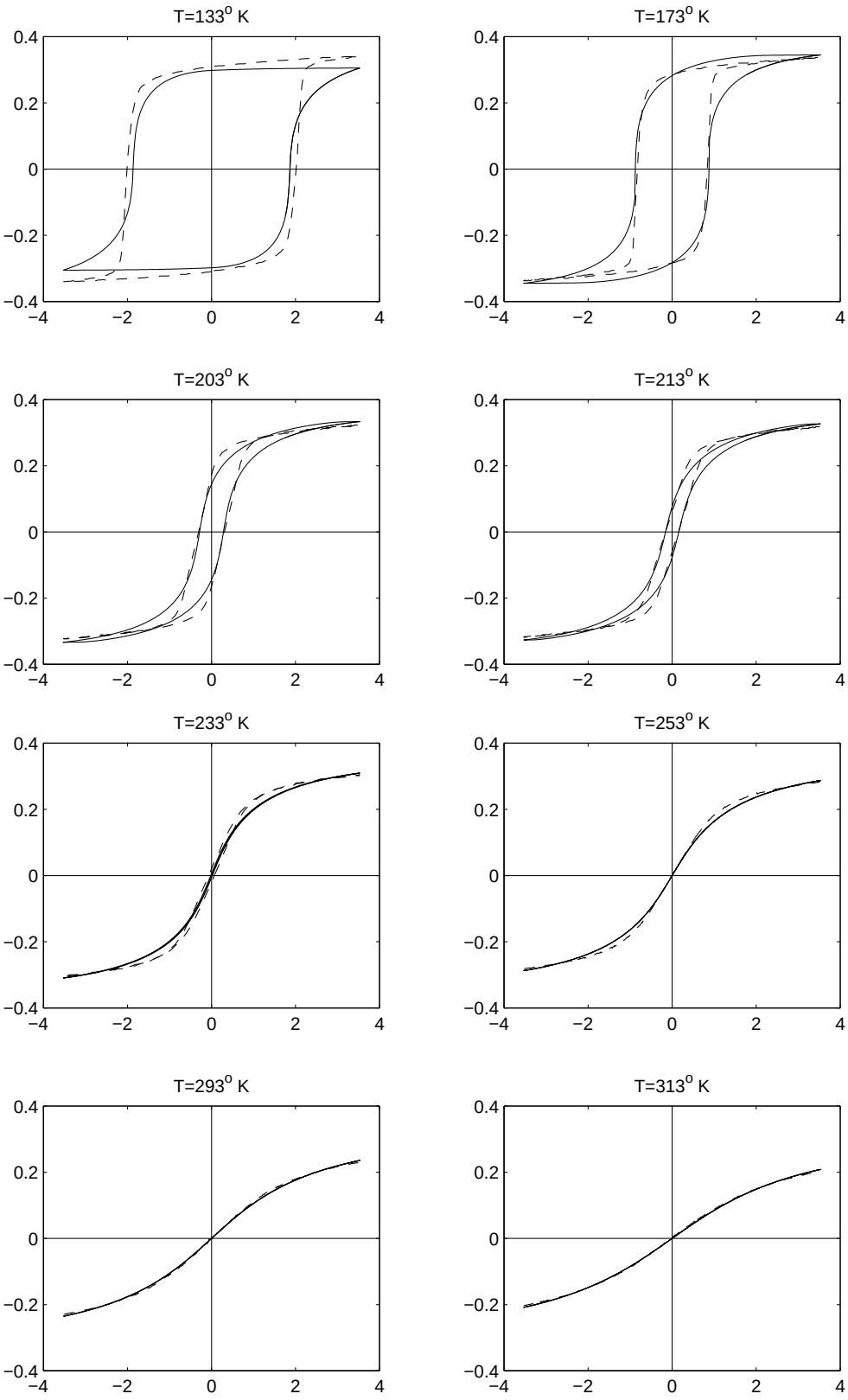

Figure 9. PMN data (– – –) from Glazounov et al. [7] and domain wall model (——) for the temperature range $T = 133^o$K to $T = 313^o$K. Abscissas: electric field (MV/m), ordinates: polarization (C/m^2).

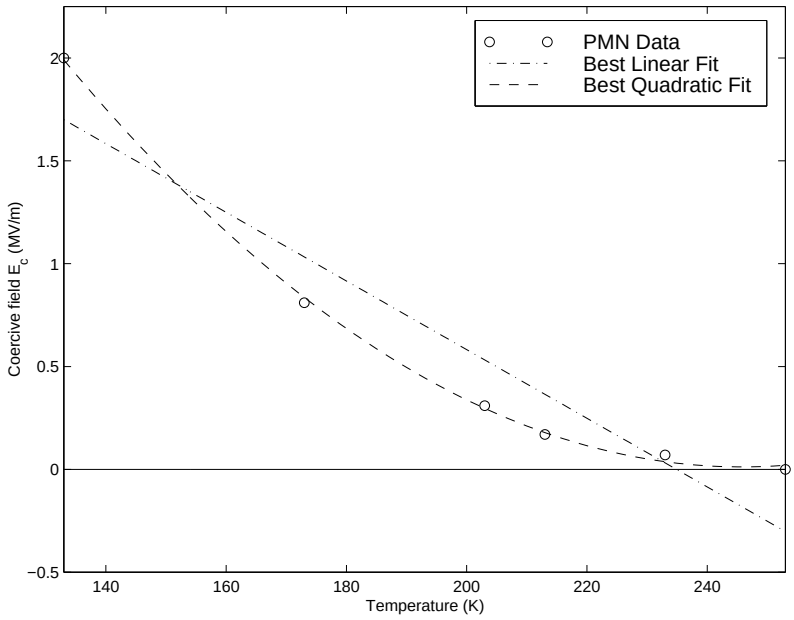

Figure 10. Coercive PMN data from Glazounov et al. [7] plotted as a function of temperature and the best least squares linear and quadratic fits to the data.

5 Concluding Remarks

This paper addresses the modeling of temperature-dependent constitutive nonlinearities and hysteresis in relaxor ferroelectric materials. As in the fixed-temperature case, the model is constructed in two steps: (i) the modeling of the anhysteretic dielectric behavior through Boltzmann and thermodynamic principles, and (ii) the modeling of hysteresis through the quantification of energy required to bend and translated domain walls pinned at inclusions inherent to the materials. The microscopic anhysteretic model is based on the assumption that the materials are comprised of micropolar regions having a broad spectrum of Curie temperature due to their chemical heterogeneity. Consideration of the free energy in the presence of variations in cation distributions yields an Ising spin model representing the thermodynamics of the microregions. Based on a "random layer" model for B-site orientations, this then provided a mechanism for computing the saturation polarization and distribution of micropolar regions as a function of temperature. A nonlinear model characterizing the aggregate material behavior, in the absence of hysteresis, was then obtained by combining the micropolar model with macroscopic constitutive relations. To quantify the hysteresis inherent to the materials at low temperatures, the energy required to reorient dipoles, and hence move domain walls, was quantified as a function of temperature. The resulting combined model characterizes the hysteresis and constitutive nonlinearities exhibited by the materials from low temperature ferroelectric regimes through the superparaelectric phase where the materials exhibit saturation effects but negligible hysteresis.

The predictive capabilities of the model were illustrated through comparison with PMN and PMN-PT-BT data collected under quasistatic conditions. For both data sets, the model quantifies the hysteresis observed at low temperatures as well as the decrease in hysteresis which occurs as temperatures increase. It also quantifies the transition to anhysteretic behavior and the reduction in saturation polarization which occurs as temperatures increase. The full temperature and field dependence is incorporated in the model and the differing model responses were obtained with one set of parameters. The sole inputs to the model

are the input field and the operating temperature. The small number of parameters (7) and their asymptotic relation to measurable quantifies (e.g., coercive field E_c, slope at field reversal) facilitates the construction of the model as well as the updating of parameters to accommodate changing operating conditions.

Due to the focus of the paper on the quantification of the thermal dependence on the dielectric properties of relaxor materials, the examples were chosen to have fixed maximum field inputs and variable temperatures. The capability of the model to accommodate variable field inputs is documented for various PZT compounds in [21] through a comprehensive set of examples.

We note that the model developed here is quasistatic in nature and hence does not yet incorporate the physical mechanisms which produce certain frequency effects in relaxor materials. Care should thus be exhibited if the model is employed in variable or high frequency regimes. While certain choices for parameters may produce accurate model fits at fixed high frequencies, this should be attributed to the mathematical flexibility of the model rather than incorporated physics. The development of a commensurate physics-based dynamical model is under current investigation.

Finally, the ODE nature of the model makes it amenable to inversion through the consideration of a complementary ODE in a manner analogous to that described in [17]. This facilitates the construction of an inverse compensator which can be used for linear control design [24, 27]. The application of these techniques for linear control implementation for piezoceramic actuators which exhibit hysteresis is also under investigation.

Acknowledgements

The authors sincerely thank A.E. Glazounov for detailed discussions regarding aspects of the model and for providing the PMN data employed in Example 2. The breadth of temperatures and dielectric behavior spanned by this data both motivated mechanisms for expanding the scope of the model and provided a means of testing the model over an extended temperature range.

The research of R.C.S. was supported in part by NASA Grant 533155 and by the Air Force Office of Scientific Research under the grant AFOSR-F49620-98-1-0180.

References

[1] M.A. Akbas and P.K. Davies, "Domain growth in $Pb(Mg_{1/3}\ Nb_{2/3})O_3$ perovskite relaxor ferroelectric oxides," *J. Am. Ceram. Soc.*, 80(11), pp. 2933-2936, 1989.

[2] S.A. Brown, C.L. Hom, M. Massuda, J. Prodey, K. Bridger, N. Shankar and S.R. Winzer, "The electromechanical behavior of a $Pb(Mg_{1/3},Nb_{2/3})O_3$-$PbTiO_3$-$BaTiO_3$ relaxor ferroelectric: An experimental and analytical study," *J. Am. Ceram. Soc.*, 79, pp. 2271-2282, 1996.

[3] J. Chen, H.M. Chan and M.P. Harmer, "Ordering structure and dielectric properties of undoped and La/Na-doped $Pb(Mg_{1/3}\ Nb_{2/3})O_3$," *J. Am. Ceram. Soc.*, 72(4), pp. 593-598, 1989.

[4] I-W. Chen and Y. Wang, "A domain wall model for relaxor ferroelectrics," *Ferroelectrics*, 206, pp. 245-263, 1998.

[5] L.E. Cross, "Relaxor ferroelectrics," *Ferroelectrics,* 76, pp. 241-267, 1987.

[6] M.A. Ealey and J.F. Washeba, "Continuous facesheet low voltage deformable mirrors," *Opt. Eng.*, 29(10), pp. 1191-1198, 1990.

[7] A.E. Glazounov, A.J. Bell and A.K. Tagantsev, "Relaxors as superparaelectrics with distributions of the local transition temperature," *J. Phys.: Condens. Matter*, 7, pp. 4145-4168, 1995.

[8] A.D. Hilton, D.J. Barber, C.A. Randall and T.R. Shrout, "On short range ordering in the perovskite lead magnesium niobate," *J. Mater. Sci.*, 25, pp. 3461-3466, 1990.

[9] C.L. Hom, "Simulating electrostrictive deformable mirrors: II. Nonlinear dynamic analysis," *Smart Mater. Struct.,* 8, pp.700-708, 1999.

[10] C.L. Hom, P.D. Dean and S.R. Winzer, "Simulating electrostrictive deformable mirrors: I. Nonlinear static analysis," *Smart Mater. Struct.,* 8, pp.691-699, 1999.

[11] C.L. Hom and N. Shankar, "A fully coupled constitutive model for electrostrictive ceramic materials," *J. Intell. Mater. Sys. Struct.*, 5, pp. 795-801, 1994.

[12] C.L. Hom and N. Shankar, "Modeling nonlinearity in electrostrictive sonar transducers", *J. Acoust. Soc. Am.*, 104(4), pp. 1903-13, 1998.

[13] C.L. Hom and N. Shankar, "A constitutive model for relaxor ferroelectrics," Proceedings of the SPIE, Newport Beach, CA, 1999.

[14] U.F. Kocks, A.S. Argon and M.F. Ashby, *Thermodynamics and Kinetics of Slip*, Volume 19 in *Progress in Materials Science*, B. Chalmers, J.W. Christian and T.B. Massalsk, Eds., Pergamon Press, Oxford, 1975.

[15] S.M. Pilgrim, M. Massuda, J.D. Prodey, and A.P. Ritter, "Electrostrictive sonar drivers for flextensional transducers," *Transducers for Sonics and Ultrasonics*, Eds., M. McCollum, B.F. Hamonic, and O.B. Wilson, Lancaster PA, Technomic, 1993.

[16] N. Shankar and C.L. Hom, "An acoustic/thermal model for self-heating in PMN sonar projectors," *J. Acoust. Soc. Am*, submitted.

[17] R.C. Smith, "Inverse compensation for hysteresis in magnetostrictive transducers," CRSC Technical Report CRSC-TR98-36; *Mathematical and Computer Modeling*, to appear.

[18] R.C. Smith, C. Bouton and R. Zrostlik, "Partial and full inverse compensation for hysteresis in smart material systems," Proceedings of the 2000 American Control Conference, to appear.

[19] R.C. Smith and C.L. Hom, "A domain wall model for ferroelectric hysteresis," SPIE Conference on Mathematics and Control in Smart Structures, SPIE Volume 3667, Newport Beach, CA, March 1-4, 1999, pp. 150-161.

[20] R.C. Smith and C.L. Hom, "Domain wall theory for ferroelectric hysteresis," *J. Intell. Mater. Sys. Struct.*, 10(3), pp. 195-213, 1999.

[21] R.C. Smith and Z. Ounaies, "A domain wall model for hysteresis in piezoelectric materials," CRSC Technical Report CRSC-TR99-33; *J. Intell. Mater. Sys. Struct.*, to appear.

[22] R.C. Smith and R. Zrostlik, "Inverse compensation for ferromagnetic hysteresis," CRSC Technical Report CRSC-TR99-28; Proc. 38th IEEE Conf. Dec. and Control, Phoenix, AZ, 1999.

[23] G.S. Smolensky, "Physical phenomena in ferroelectrics with diffused phase transition," *J. Phys. Soc. Jpn. (Suppl.)*, 28, pp. 26-37, 1970.

[24] G. Tao and P.V. Kokotović, *Adaptive Control of Systems with Actuator and Sensor Nonlinearities*, John Wiley and Sons, New York, 1996.

[25] D. Viehland, S.J., Jang, L.E. Cross, M. Wutting, "Deviation from Curie-Weiss behavior in relaxor ferroelectrics," *Phys. Rev.*, 46(13), pp. 8003-8006, 1992.

[26] D. Viehland, S.J. Jang and L.E. Cross, "Freezing of the polarization fluctuations in lead magnesium niobate relaxors," *J. Appl. Phys.*, 68(6), pp. 2916-2921, 1990.

[27] B. Widrow and E. Walach, *Adaptive Inverse Control*, Prentice Hall, NJ, 1996.